Proceedings of Montreal 2018
Global Power and Propulsion Forum
7th – 9th May, 2018
www.pps.global

GPPS-NA-2018-113

Intake Geometry and Shear Layer Ingestion Effects on Embedded Propelling Fan Performance

Theofilos G. Efstathiadis
Laboratory of Fluid Mechanics and Turbomachinery, Department of Mechanical Engineering, AUTH
theofil@auth.gr
GR-54124, Thessaloniki, Greece

Vasilis G. Gkoutzamanis
Laboratory of Fluid Mechanics and Turbomachinery, Department of Mechanical Engineering, AUTH
vgkoutzam@meng.auth.gr
GR-54124, Thessaloniki, Greece

Michalis E. Vourakis
Laboratory of Fluid Mechanics and Turbomachinery, Department of Mechanical Engineering, AUTH
vourakis.term@gmail.com
GR-54124, Thessaloniki, Greece

Anestis I. Kalfas
Laboratory of Fluid Mechanics and Turbomachinery, Department of Mechanical Engineering, AUTH
akalfas@auth.gr
GR-54124, Thessaloniki, Greece

ABSTRACT

This work presents an experimental investigation for the effects of three-dimensional flow phenomena, which unfold at boundary layer ingestion (BLI) aero-engine intakes of S-shaped geometry, on the performance of a one-stage multi fan compressor unit.

The experimental setup consists of two groups of fans: the first one simulates the cruise velocity, while the second one constitutes the compressor unit. Three cases are examined: a straight duct intake as the baseline case and two S-shaped cases. The variable parameter which alters through an inherent mechanism is the length over height ratio (L/H) that characterizes the intake geometry.

Oil and dye visualization method is used at the suction area upstream of the compressor unit array for the various intake shapes. Total and static pressure measurements are also performed at the aerodynamic interface plane (AIP) and cross section areas across the intake. This is achieved with a pneumatic five-hole probe which is built and calibrated at the Laboratory of Fluid Mechanics and Turbomachinery of Aristotle University of Thessaloniki (AUTH).

The results of the flow visualization, show that the transition of intake geometry from a straight duct towards S-shaped aggressive geometries of decreasing L/H ratios, causes a movement of the saddle points upstream and an enlargement of corner vortices. Pneumatic measurements at various cross-section areas across the S-duct focusing on the central fan, reveal increasing energy losses and verify the existence of counter rotating vortices, especially when the more aggressive intake is used (lower L/H). Additionally, the maximum flow angles are achieved at the most aggressive geometry. The isolation of the suction area of the fan from the flow above it, is the most intense. Furthermore, although distortion effects, are maximized upstream of the compressor array for geometries of higher offset, compression ability of the fan at proximate cross section areas, is not affected as compared to the straight duct.

Finally, the significant drop in mass flow rate for the side fans which is associated to the counter rotating vortices, has a major impact on the engine peformance. Comparing the performance of the corner fans to that of the central fan, indicates a reduction of more than 20%, for the former.

INTRODUCTION

The Aviation Industry has nowadays made tremendous strides in increasing the aircraft's efficiency. This is mainly realized by significantly reducing the fuel consumption of the aero-engines. However, the number of commercial aircraft and the number of people flying every day is expected to double by 2036. At the same time, the cost per gallon of aviation fuel is expected to triple (NASA, 2017). The ACARE Flightpath 2050 (European Commission, 2011) has set some

specific goals regarding aviation sustainability, in order to further reduce aircraft fuel demands and limit the pollutant emissions from civil aircrafts. These goals mainly demand a considerable CO_2 (90%) and NOx (65%) reduction which can be attained by introducing major technological aviation breakthroughs.

These breakthroughs mainly target in aerodynamic drag reduction and more efficient aero engine operation, which can be achieved in many ways. One of these ways is to investigate integrated aircraft concepts. These include the study of the interaction of the jet's wake and aircraft's body as a whole. The development of more efficient computational and experimental tools as well as new materials allows for new design concepts with embedded propulsive units onto/into the aircraft's body. The characteristics of the embedded engines as compared to the conventional engines are presented in Table 1 .

Table 1 Characteristics of embedded engine propulsion systems (Sharma, 2015)

Advantages	Disadvantages
Elimination of engine pylons → reduced weight and drag	Low energy boundary layer air ingestion → lower thrust
Elimination of fan diameter limitations → high BPR fans with possible noise reduction	Non-uniform flow pattern and S-duct configuration → degradation of inlet performance
Elimination of a non-lifting fuselage	Distortion at the fan inlet → higher specific fuel consumption and vibration
Fuselage exposed surface area savings	More sophisticated design is required
BLI drive to fuel burn benefits	Unproven technology

Towards this direction, NASA and Boeing are studying many distributed propulsion systems, which lead to performance improvement and noise reduction. The utilization of redundant engines, but of reduced size compared to the conventional ones, significantly reduces noise and among other advantages (Ko *et al*., 2003), it offers improved safety (Leifsson *et al*., 2013).

One concept that is increasingly investigated over the last two decades and is proposed by NASA, is the Blended-Wing-Body (BWB) system. Transitioning to such conceptual designs may lead to remarkable performance improvements over conventional aircrafts, such as 15% reduction in takeoff weight and 27% reduction in fuel burn per seat mile (Liebeck, 2004). In BWB aircrafts, the system is studied as a whole which means that no distinction exists between the wings and the fuselage. Placement of the propulsion system in a BWB can be done in two ways; the podded and the embedded engine configuration. The latter, which is investigated throughout this work, requires the use of Boundary Layer Ingestion (BLI) inlets through S-ducts.

Due to the non-uniform pressure profile and low momentum of the inserted flow the studying of the inlet geometry for BLI is of great importance. This distortion at the Aerodynamic Interface Plane (AIP) represents the major issue for the engine's efficiency reduction (Ferrar and O'Brien, 2012).

The experimental study of the interaction between the three-dimensional flow phenomena and the intake geometry, consists the major purpose of this investigation. Its motivation lies in the potential of designing embedded engines in this way to improve fuel economy and reduce emissions and noise of future aircrafts. The main challenge imposed is the heterogeneous flow regime that is realized at the engine's intake. Major focus is placed on the central fan of the experimental setup.

METHODOLOGY

The experimental methods applied are conducted in two parts. The first part focuses on the flow visualization of the phenomena and the second one, consists of pressure measurements that focus on the central fan. Both parts are conducted in the suction area upstream of the compressor array and on various cross sections of the intake duct.

Experimental Setup

The experimental setup, as shown in Figure 1, is an open circuit wind tunnel and is designed and built at the Laboratory of Fluid Mechanics and Turbomachinery (LFMT) of Aristotle University of Thessaloniki (AUTH) (Efstathiadis *et al*., 2017).

The various parts target to accurately simulate a BLI system through an S-shaped intake. The first constituent is the fan box that comprises of 10 axial fans. Its role is to simulate the cruise velocity (V_∞) and produce the required air mass flow. The second element of the experimental setup is a honeycomb flow straightener combined with screen, placed downwards of the fan box. Its role is to remove the swirl induced from the rotors. Moreover, in order to guide the axial and vertical movement of the S-shape filament, a horizontal plate is placed after the flow straightener. The following component is the S-shape filament, with one of its sides attached to the horizontal plate.

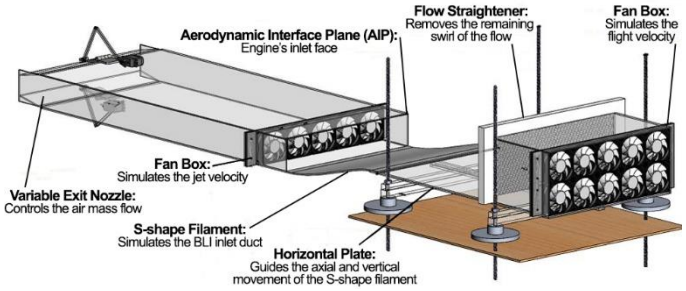

Figure 1 Experimental set up for the investigation of the geometry effects on the boundary layer ingestion (Efstathiadis *et al*., 2017)

The system described so far, (fan box, flow straightener, horizontal plate and one of the S-shaped filament sides) provides the ability to adapt the height (H) and length (L) of the inlet geometry. For the simulation of the S-duct, a poly-vinyl-chloride (PVC) sheet of 1mm thickness is used, due to its flexibility.

Furthermore, the second fan box constitutes the compressor unit and consists of a 5-fan array that simulates the engine's jet velocity V_j. The geometric positioning of the compressor fan array simulates the embedded propulsive unit with regard to the fluid flow direction. Regarding the selection of the fan box rotational speed it is selected to be the maximum possible to provide a homogeneous flow at the intake. Therefore, the first stage (10-fan array) is characterized by a rotational speed of 5200 rpm while the second stage (5-fan array) is running with 5400 rpm. The rotating speed is controlled throughout the entire process with effectively used speed sensors and the induced errors from the experiments are assumed acceptable as these are below 3%.

Finally, a variable nozzle is placed at the end of the setup in order to control the air mass flow that is allowed through the aerodynamic interface plane (AIP). For the conduction of the present experiments, the nozzle's geometry is orthogonal with the same cross section as the orthogonal duct that is placed downwards of the second fan box.

In order to perform the experiments, the geometry of the S-shaped intake has to be defined. The selection of the intake geometries is of vital importance as it is the main variable parameter of this study. It is based on using L/H ratios which correspond to real S-shaped aero-engine intake architectures. Taking into consideration the above and in combination with the available measuring equipment, three different cases are examined as shown in Figure 2. The first one is the reference case (baseline case) with a straight duct configuration.

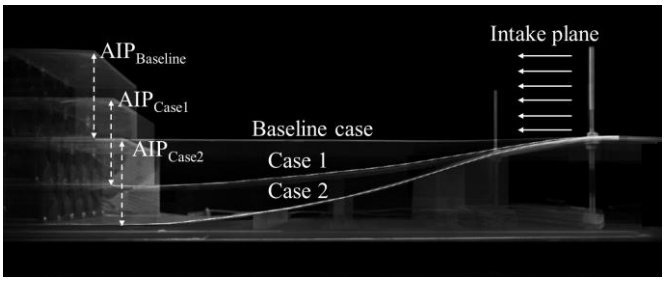

Figure 2 Investigated geometries

The two following cases consist of S-shaped geometries which are adapted by adjusting the horizontal plate as described in the 'experimental setup' section. In this way, the geometry is converted from a mild geometry (Case 1) to an aggressive one (Case 2). Case 1 is placed in such a way so that the fans' shafts (center of AIP_{Case1} plane) are at the same height with the S-shaped intake plane. Case 2 is formed by placing the compressor fan array in such a way that the top of the AIP_{Case2} is at the same height with the S-shaped intake plane. The resulting offsets (L/H ratios) are the following:

- Case 1 → L/H = 6.42
- Case 2 → L/H = 4.11

Visualization Technique

In cases where identification of the examined stream lines is required, surface visualization methods are deemed appropriate. This technique is widely used as a preliminary tool that allows for the identification of the physical sizes and locations of the flow features under consideration. For the purposes of this work, the oil and dye visualization method is used at the suction area upstream of the compressor unit for the various intake shapes. These are simple flow visualization experiments, relatively inexpensive and provide an accurate perception of the flow domain (Terzis *et al*., 2011).

When using the oil and dye technique, particular attention must be paid to the mixture quantity. Due to the small flow speed used in the experiments a very thin mixture is needed, so that it can be carried away by the air flow. However, this is achieved with extreme difficulty, if only oil is used (Welborn *et al*., 1992). Thus, a small quantity of colored molecules is mixed with almost equal quantity of thin molecule oil, so that a luminous, homogeneous mixture is created as it is also shown in the 'Results and Discussion' section (Figure 4). The rest of the oil is added in small quantities to the mixture, combined with solvent, until the desired concentration is achieved. The solvent greatly diminishes the viscosity of the mixture. The smaller the free-flow speed, the more solvent is needed for dilution so that the mixture becomes thinner. In flow speeds greater than 12-14 m/s, a mixture consisting only of oil and color pigments is most appropriate. However, in lower speeds (< 4-5 m/s) the mixture cannot consist only of oil and color pigments. The latter case can impose problems to the experiment execution, since waveforms can be created in the examined surface, as the pure spirit can separate from color pigments. This is explained from the fact that solvent and pigments do not mix well together.

Pressure Measurements

There are complex phenomena (three-dimensional) developed in embedded engine configurations with BLI in S-shaped intakes. Hence, in order to comprehend and analyze them, both magnitude and direction must be defined to measure velocity components. For this reason, a pneumatic five-hole probe (Figure 3) has been calibrated in LFMT, to measure total and static pressure as well as to provide means of calculating the flow's main angles for the calculation of the velocity components.

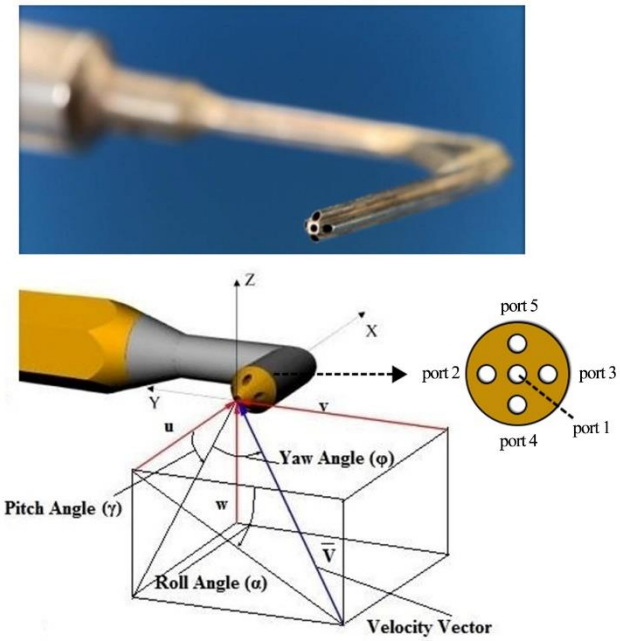

Figure 3 Five-hole probe used in pressure measurements

All pressure measurements are combined with a pneumatic pressure scanner (Netscanner 9116) and an engineering software for data acquisition. The full-scale measurement accuracy of the pressure scanner is 0.05%. The probe is manufactured by stainless steel. Its tip diameter is as small as 1.45mm, ensuring a minimally invasive and highly accurate method for the investigation of the flow. Once the flow angles are measured and combined with the flow speed magnitude, the direction of the flow is defined. The calibration method employed for the conduction of this study is the non-nulling mode, and is performed at a small, open-type suction wind tunnel. This type of calibration is widely adopted and requires that the pressure probe is exposed to a steady, uniform flow field of known properties and fixed direction. Whenever it is employed in such flow field, the probe is rotated at a previously defined set of angle combinations (pitch [γ] and yaw[φ]) that cover the range of incidence angles that are expected for the probe to encounter during the actual tests. At every angle combination point, the pressures of the five holes are measured, resulting into a pressure data matrix from which the calibration and pressure coefficients can be calculated aiming to data reduction. The calibration method is thoroughly provided in the works of Magkoutas *et al*. The method is based on the Treaster and Yocum algorithm (Treaster and Yocum, 1978). Based on this, the following dimensionless coefficients are calculated as follows:

Yaw angle $$K_{yaw} = \frac{P_3 - P_2}{P_1 - P_{aver}} \quad (1)$$

Pitch angle $$K_{pitch} = \frac{P_5 - P_4}{P_1 - P_{aver}} \quad (2)$$

Total pressure $$K_t = \frac{P_1 - P_{tot}}{P_1 - P_{aver}} \quad (3)$$

Static pressure $$K_s = \frac{P_{aver} - P_{st}}{P_1 - P_{aver}} \quad (4)$$

i-th hole (i stands for ports 1-5) $$Cp_i = \frac{P_i - P_{ref}}{P_1 - P_{aver}} \quad (5)$$

Where P_{aver} is the mean of the pressures measured by the side holes:

$$P_{aver} = \frac{P_2 + P_3 + P_4 + P_5}{4} \quad (6)$$

RESULTS AND DISCUSSION

This section provides the results that arise from both visualization and pressure measurements conducted in the experimental setup described above.

Visualization Results

The purpose of using the oil and dye visualization techniques for the selected S-shaped geometries is to reveal the relation of three-dimensional flow phenomena and the intake geometry, at the AIP (outlet of the S-shaped duct). Its goal is to locate and record the saddle points and corner vortices at the suction area upstream of the second fan box array (compressor unit).

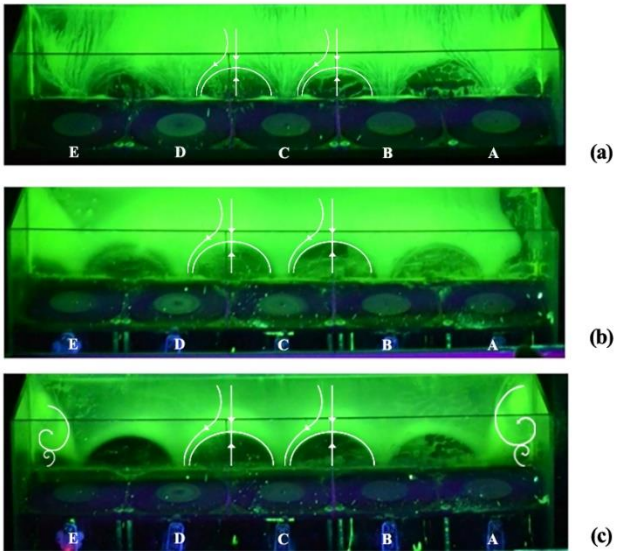

Figure 4 (a) Baseline case, (b) mild geometry, (c) aggressive geometry

Figure 4 depicts the three examined cases (Letters A to E correspond to each fan of the second box). It can be observed that the intensity of the flow phenomena changes as we progress from the baseline case (a) to the aggressive S-duct geometry (c). The suction field of the corner fans is dominated by counter rotating vortices that form recirculations. These vortices emanate from the boundary layer detachment near the wall that surrounds the fans and leads to flow blockage and total pressure reduction upstream of the fan. Also, the larger vortices that are shown in Figure 4 are followed by smaller, counter rotating vortices. As the L/H ratio is decreased, the size of corner vortices increases.

Moreover, regarding the saddle points, these are formed at points where, opposite (upstream and downstream to the points) moving streamlines meet. The first stream line follows the main flow direction that simulates the cruise velocity, while the second stream moves on the opposite direction due to its strike on the fan casing. According to the visualization experiments, it is observed that as the offset of the intake increases (L/H reduction), the saddle points move upstream. The overall described observations (recirculations, mass flow reduction) have a clear effect on the overall efficiency of the system as they induce losses. In particular, moving to a more aggressive geometry (lower L/H) leads to efficiency reduction due to smaller available suction area upstream the fans which leads to decreased air mass flow.

In order to extract the profile of the flow field and be able to compare it with a theoretical model, a computational tool is developed using Matlab. This model consists of a fifth-degree polynomial, using a regression tool to reproduce the total saddle points and the corner vortices. The optimization parameters used are the root sum squared (RSS) method and coefficient of determination R^2 (Figure 5).

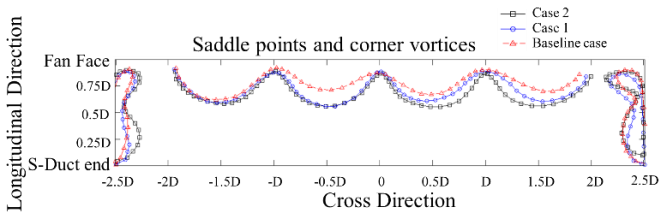

Figure 5 Profile extraction of the saddle points and corner vortices for the three cases

Despite that the flow is expected to be fully symmetric theoretically (capability of the second fan box to operate in the same rpm), visualization experiments demonstrate that there are larger vortices on the right side of the graph (cross direction) and an asymmetry of the flow field is revealed. For this reason, even that visualization leads to rapid observations of the phenomena, more accurate experiments are needed to better describe the flow behavior for the different intake geometries. Therefore, the analysis advances to pressure measurements that are characterized by a higher degree of accuracy.

Pressure Measurement Results

Pressure Measurements at Aerodynamic Interface Plane

The first part of pressure measurements is conducted in the AIP in order to verify the visualization results, such as the asymmetrical flow field. The operating conditions both for the visualization and the pressure measurements are identical (rpm, nozzle configuration). The five-hole pneumatic probe is used to measure total and static pressure. It is attached onto a cantilevered mechanism, able to move both on the vertical (Z) and cross (Y) direction.

The measurement grid consists of 1377 points (81x17) and is selected based on the available time so that measurements are completed within a day and ensure that operating conditions remain the same. The time interval of 30 seconds is employed. The 81 points are located on the Y-axis (cross direction) while the 17 points are placed on the Z-axis (vertical direction) (Figure 6).

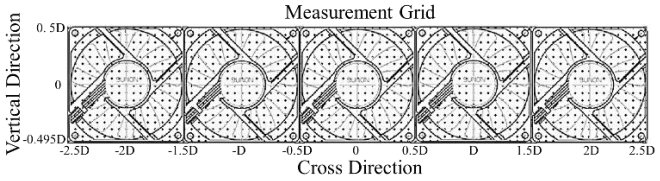

Figure 6 Measurement grid upstream of the compressor array

The results presented here are based on the aggressive geometry (Case 2). Figure 7 represents the dimensionless, total pressure distribution on the AIP. Point '0' represents the symmetry line of the central fan. Points 'D" and '-D' represent the symmetry line of the eccentric fans that are placed next to the central fan, while points '2D' and '-2D' represent the symmetry line of the corner fans. The letter D represents the outer diameter of the selected fans.

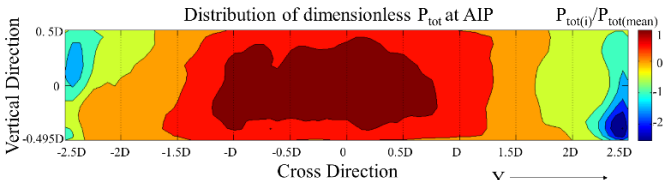

Figure 7 Total pressure distribution at AIP

At this point, a significant heterogeneity appears on the suction side upstream of the fan array. It is observed that the central fan's total pressure distribution dominates over the side and corner fans. The pressure field is almost symmetrical compared to the asymmetric behavior that is measured for the side fans. The low-pressure area from 1.25D to 2.5D (and -1.5D to -2.5D respectively) is associated to the counter rotating vortices that generate recirculations near the wall upstream the fan box and hence induce a reduction in the mass flow. This is also observed and explained in the visualization part. Comparing the performance of the corner fans to the one of the central fan, indicates a reduction of more than 20%, for the corner fans.

Moreover, according to static pressure measurements, a similar heterogeneity appears regarding the part of the flow at the two corners of the fan array. The dimensionless static pressure distribution (Figure 8) of the right corner fan is characterized by larger areas of maximum values, as compared to the left corner fan. This verifies the significant heterogeneities of the corner fans. Regarding the central fan, it is characterized by symmetric flow field.

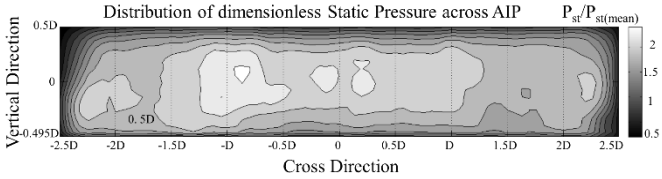

Figure 8 Static pressure distribution at AIP

After having described the fundamental parameters that can also be measured by a Pitot-Static tube, the major advantage of using a five-hole probe is that it allows for the investigation of the flow angles' direction. This applies for the yaw and pitch angles that provide information for the X-Y and X-Z planes.

Figure 9 represents the distribution of pitch angle at AIP. The flow field of the central fan is characterized by an overall symmetry. There are two areas of interest here. The area of the corner fans and the area of the upper part of the fans.

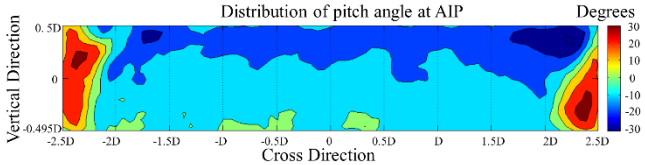

Figure 9 Pitch angle distribution at AIP

Regarding the area of the corner fans and given the angle range and the existence of vortices (observed in the visualization part), the measured values of the flow angles are not deemed accurate. However, they verify the existing

heterogeneity on the corner fans. Regarding the latter, the flow angles that are observed (-20°) are associated to the fans' suction from the surrounding environment. This is explained due to the existence of the S-shaped filament (Case 2). The main flow avoids the adverse pressure gradient which is due to the geometry of the S shaped intake and travels above the second fan array. Hence, as the fans are fed insufficiently by the flow, they are constrained to draw air from the main flow that travels above the upper part of the fans.

Regarding the distribution of yaw angle at AIP, figure 10 depicts what is also observed in the static pressure figure. The flow has the tendency to move to the left, regarding the central and the two eccentric fans.

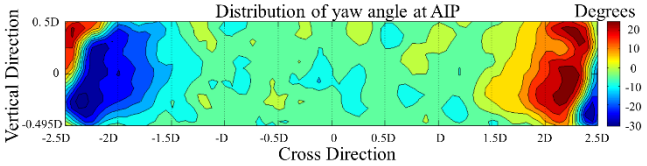

Figure 10 Yaw angle distribution at AIP

The corner fans are characterized by the greatest maximum and minimum values of angles which also lead to the conclusion that they may not be considered as reliable.

To sum up, the abovementioned measurements indicate the capabilities of the presented five-hole probe to measure the largest part of the flow field, with the exception of the two corners of the array. Due to the measured symmetry of the central fan, the focus is placed on its behavior in the following section. In this way, both the measuring capabilities of the probe (measured flow angles are within the acceptable range), as well as the easier correlation of the geometry variation and the flow field can be exhibited.

Pressure Measurements at Various Cross-Section Areas Across the S-duct

The second part includes pressure measurements focusing on three cross sections upstream of the central fan, which can be observed in Figure 11. These are located at the starting point of the S-shaped intake, the middle point and the end-point of the intake respectively. The measurement grid is also observed in Figure 11 and consists of 1080 points (40x27). The conditions are kept the same as in the previous measurement configuration (rpm, cross-section of the outlet nozzle and time intervals of measurements).

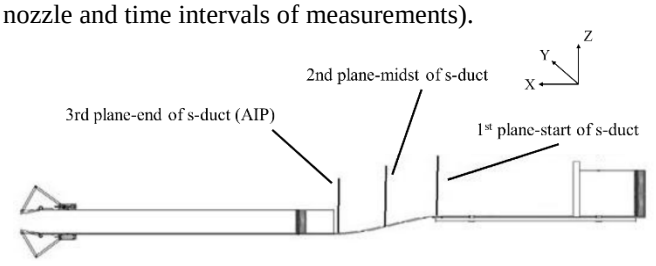

Figure 11. Cross-sections of measurements on the S-shape geometries

In the same manner as in the previous section, the dimensionless total pressure distribution at the three planes is provided. The quantity used for the nondimensionalization is

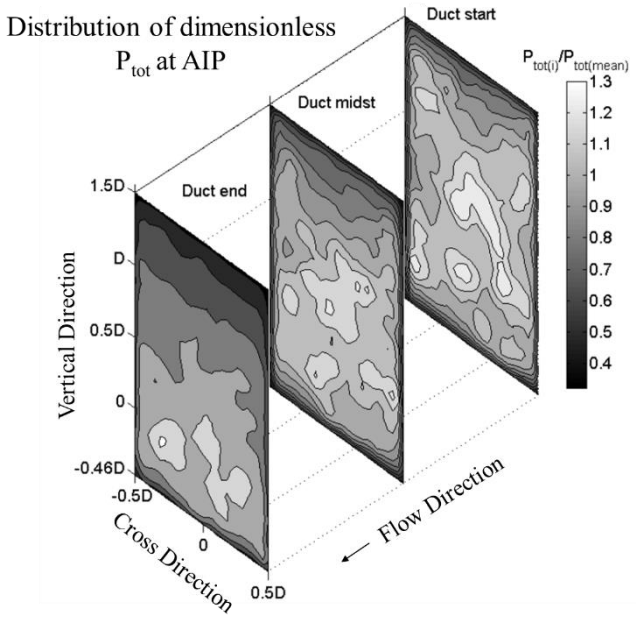

Figure 12 Total pressure distribution at three planes of measurement for the baseline case

the mean total pressure of the measurement plane. Measurements are initially conducted for the baseline case (Figure 12). The natural flow deployment from the starting, to the middle section is observed. Maximum pressure values are distributed at the center of the cross-sections. A small pressure reduction is measured for the midst section which is expected, due to the distance covered by the flow in the duct. This is intense at the upper part of the grid due to the flow diffusion to the surrounding environment. Moving on to the straight duct end plane, a clear stratification is observed (for values greater than 0.5D – vertical) which further extends to lower values up to 'D' point. Below that area and up to the height of 0.5D, further development of the flow is affected by diffusion, due to reduced values of total pressure, compared to the

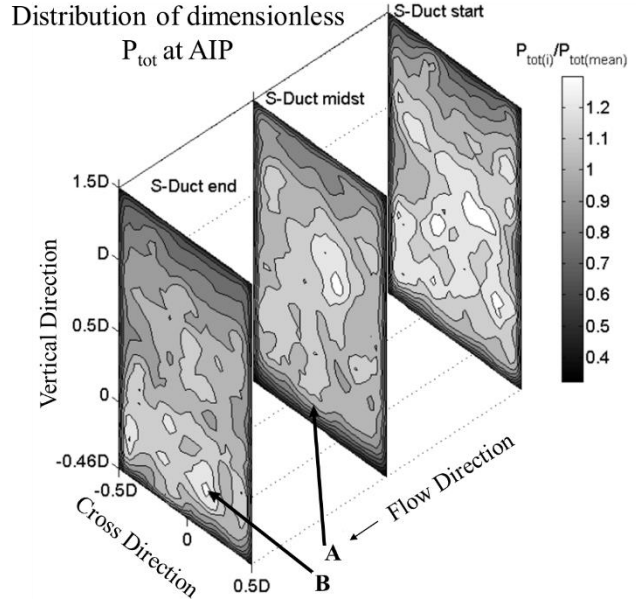

Figure 13 Total pressure distribution at three planes of measurement for the mild S-duct (Case 1)

respective areas of the previous cross-sections. The area upstream the measured cross-section presents an increased distribution compared to the respective area of the midst section, as the compressors add energy to the flow. Additionally, all three planes are characterized by symmetric flow field.

The second case is characterized by an S-shaped intake with a mild configuration (Case 1). Once again, the dimensionless total pressure for the three planes of measurement is shown (Figure 13).

As compared to the baseline case, pressure measurements show that maximum pressure values are displaced to lower levels (negative Z-direction). In the midst section, the maximum pressure values are displaced to the positive vertical direction, due to the position of the midst cross-section which is placed at a lower height. This is also confirmed by the diffusion reduction in the upper end of this measurement plane. It is noted that the minimum pressure area is increased (vertical direction) in the presence of the adverse pressure gradient, caused by the S-shaped curvature (area A). Regarding the cross-section upstream the fans, the stratification that was observed in the baseline case is eliminated (area B). Moreover, the area of high pressure values is displaced to the right. This is the first observation of distortion effects on the flow, under the influence of the S-shaped geometry.

Regarding the aggressive geometry (Case 2), an overall total pressure reduction downstream the outlet of the S-shaped duct is observed (Figure 14). The phenomena for this geometry are more intense. The areas of maximum pressure values move upwards while the area of diffusion at the upper end of the flow field is increased caused by the reduced total pressure. The second cross-section indicates an area of maximum pressure which moves upwards, due to the displacement of the measurement grid's height, as compared to the S-duct intake plane. The minimum pressure area is further increased (area A) while in the area upstream of the fans, a separation of the field is observed (area C). Additionally, the area of high pressure values is further displaced to the right (area B).

In order to obtain a clear comparison of the three intake geometries, the average pressure profiles have been computed as a function of the mass flow, for the three cross-sections, in the two directions (vertical, cross) (Figure 15).

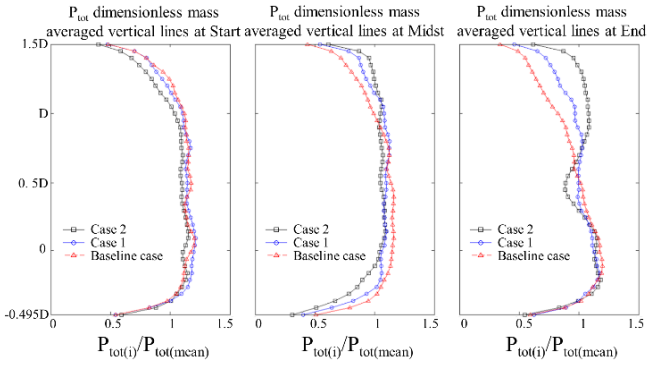

Figure 15 Vertical profiles of dimensionless total pressure at the three cross-sections (all cases)

The reduction of the total pressure as the geometry changes to more aggressive configurations, is observed for the starting cross-section. The same is observed also for the middle cross-section with the exception of the area that is located above point 'D' which is explained by the displacement of the measurement grids upwards. The third cross-section indicates the total pressure losses that are induced in the suction area (0.5D) and its recovery in lower heights. This case clearly depicts the homogeneities and heterogeneities that arise in the case of S-duct intakes. Regarding the static pressure measurements, the conclusions that occur are similar to those already described for the total

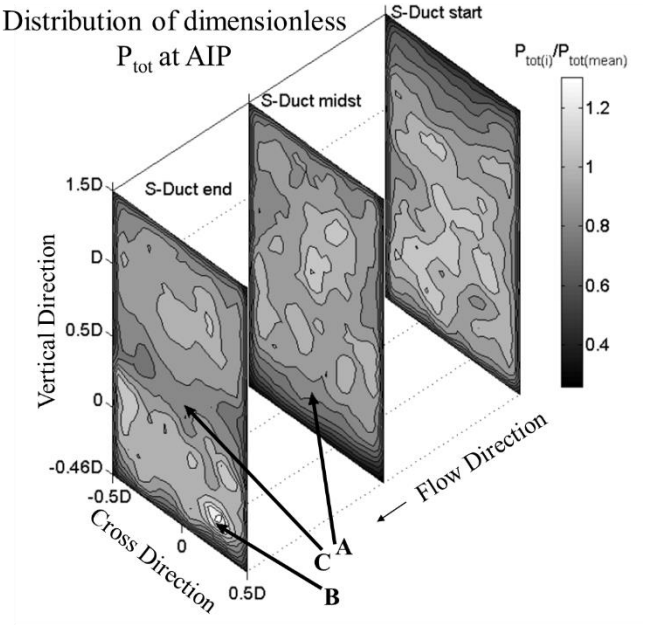

Figure 14 Total pressure distribution at three planes of measurement for the aggressive S-duct (Case 2)

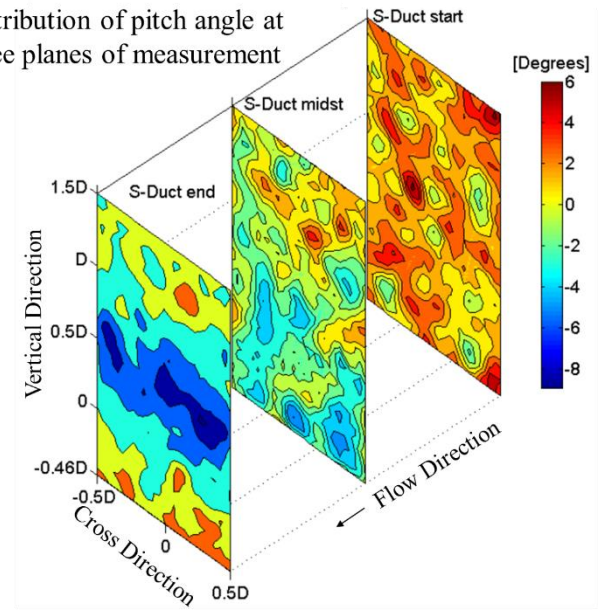

Figure 16 Pitch angle distribution at three planes of measurement for the aggressive S-duct (Case 2)

pressure measurements. Transitioning to intakes of larger offsets lead to increased energy losses.

The final part that is addressed in this investigation is the analysis of the secondary flows.

Therefore, the results of the flow angles (pitch, yaw) and velocity components are acquired for all three intake geometries. The pitch angle (Figure 16) reveals an increased flow angle range as the geometry changes to aggressive configuration. This is observed for all cross-sections that are studied. The aggressive geometry demonstrates even from the starting cross-section of measurements that they tend to have greater negative angles. The majority of positive flow angles is associated to the flow diffusion to the environment. The points of negative angles which are adjacent to areas with maximum positive angles may potentially lead to secondary flow generation.

The second flow angle that characterizes secondary flow field is the yaw angle. Even though the range of measured flow values were of the same size scale as with the results shown for the pitch angle, there is no evident trend of the flow, especially if compared for the three intake geometries. According to measurements acquired for the maximum (and minimum) values of yaw angle, there is an inability to correlate the flow angles with the various intake geometries.

Last but not least, according to the velocity components, the most important result emanates from the V_x velocity component (Figure 17), which is a reliable element to measure the energy addition of the fan to the flow. According to the velocity profiles of the main flow, it is observed that despite the increased variation of the flow for the aggressive geometry, the flow field returns to the same velocity values as with those measured in the mild case (Case 1).

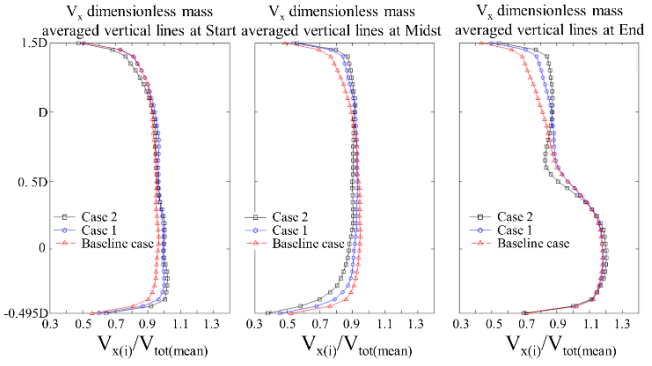

Figure 17 Vertical profiles of velocity component V_x at the three cross-sections (all cases)

CONCLUSIONS

This work presents an experimental study of a configuration that simulates the S-shaped geometry intakes of boundary layer ingesting aero-engines. The flow field developed in such cases is characterized by unsteady, three dimensional structures. The results which emerge from visualization and pressure measurements lead out to several conclusions, which are outlined as follows:

- Isolating the area upstream of the central fan results in satisfactory homogeneity. On the contrary, the suction field upstream of the side fans is intensely heterogeneous and is both observed through visualizations and measured through pressure measurements.
- Although secondary flow structures are maximized upstream of the compressor array for geometries of higher offset, compression ability of the fan at proximate cross section areas, is not affected meaning that the suction capabilities and hence the efficiency of the central fan is not affected.
- Pressure measurements show increased energy losses while transitioning to intake of larger offset (lower L/H) due to the increased inclination caused by the larger offset of the channel. The suction field of the central fan in the highest offset (L/H=4.11) is the most intense.
- The flow angle as a function of pitch and yaw angle provides an increased range of values advancing from the baseline case to S-shaped geometries. The maximum flow angles (at vertical and longitudinal direction) are achieved at the intake geometry of the highest offset.
- The suction field of the corner fans is dominated by counter rotating vortices that form recirculations. As the geometry of the intake alters to S-shaped geometries of lower L/H ratio, the size of these vortices increases in size, leading to air mass flow reduction. As compared to the performance of the central fan, the side fan performance may be reduced to more than 20%.

NOMENCLATURE

Abbreviations

AIP	Aerodynamic Interface Plane
BLI	Boundary Layer Ingestion
BWB	Blended Wing Body
LFMT	Laboratory of Fluid Mechanics and Turbomachinery

Variables

Cp	Total pressure calibration coefficient
H	S-duct inlet height [mm]
K_{yaw}	Yaw angle calibration coefficient
K_{pitch}	Pitch angle calibration coefficient
K_t	Total pressure calibration coefficient
K_s	Static pressure calibration coefficient
L	S-duct inlet axial distance [mm]
p	Pressure [Pa]

Greek

γ	Pitch angle [°]
φ	Yaw angle [°]

Subscripts

aver	Average
st	Static
tot	Total

REFERENCES

[1] Efstathiadis T., Magkoutas K. I., Ntalianis P. & Kalfas A. I., (2017). 'Geometry Curvature Effect on Boundary Layer Ingestion and Aeroengine Intake Performance',

Proceedings of 23rd ISABE Conference, ISABE-2017-22502

[2] European Commission, (2011). 'Flightpath2050 – Europe's Vision for Aviation', Report on the High Level Group on Aviation Research, ISBN 978-92-79-19724-6

[3] Ferrar, A. M. and O'Brien, W. F., (2012). 'Fan Response to Total Pressure Distortions Produced by Boundary Layer Ingesting Serpentine Inlets', 48th AIAA/ASME/SAE/ASEE Joint Propulsion Conference and Exhibit and 10th International Energy Conversion Engineering Conference, AIAA, Atlanta, doi: 10.2514/6.2012-3996

[4] Ko, A., Schetz, J. A. and Mason, W. H., (2003). 'Assessment of the Potential Advantages of Distributed-Propulsion for Aircraft', ISABE-2003-1094, Cleveland

[5] Leifsson, L., Andy Ko, William H. Mason, Joseph A. Schetz, B. Grossman, and R. T. Haftka, (2013). 'Multidisciplinary design optimization of blended-wing-body transport aircraft with distributed propulsion', Aerospace Science and Technology 25, no. 1, 16-28, doi: 10.1016/j.ast.2011.12.004

[6] Liebeck R. H., (2004). 'Design of the Blended Wing Body Subsonic Transport, Journal of Aircraft', Vol. 41, No. 1, doi: 10.2514/1.9084

[7] Magkoutas, K. I., Efstathiadis, T. G. & Kalfas, A. I., (2016). 'EXPERIMENTAL INVESTIGATION OF GEOMETRY EFFECTS AND PERFORMANCE OF FIVE-HOLE PROBE IN MEASURING JETS IN CROSSFLOW', XXII Biannual Symposium on Measuring Techniques in Turbomachinery Transonic and Supersonic Flow in Cascades and Turbomachines

[8] Magkoutas, K. I., Efstathiadis T. G. & Kalfas A. I., (2017). 'Experimental investigation of novel fuel-air premixing device for low NOx combustion', International Journal of Terraspace Science and Engineering 9(2)2017 69-77,

[9] NASA Glenn Research Center, (2017). 'Boundary Layer Ingestion Propulsion', https://www1.grc.nasa.gov/aeronautics/bli

[10] Sharma, A., (2015). 'Design of Inlet for Boundary Layer Ingestion in a Blended Wing Body Aircraft', Tech. rep., Master Thesis, Faculty of Aerospace Engineering, Delft University of Technology

[11] Terzis, A., Zachos, P., Charnley, B., Pachidis, V., & Kalfas, A. I., (2011). 'On the applicability of oil and dye flow visualization technique during the design phase and operation of experimental rigs', Journal of Flow Visualization and Image Processing, 18, 3, 199-214

[12] Treaster A. L., Yocum A. (1978). 'The calibration and application of five-hole probes', ISA Transactions 18 (3)

[13] Welborn, S. R., Reichert, B. A. and Okiishi, T. H., (1992). 'An Experimental Investigation of the Flow in a Diffusing S-Duct', AIAA-92-3622, Nashville